Breakup of positronium in a collision with a Li^+ ion

S. Roy and C. Sinha
Theoretical Physics Department, Indian Association for the Cultivation of Science, Kolkata 700032, India
(Received 31 March 2009; published 24 August 2009)

Fragmentation of ground-state ortho-positronium in collision with Li ion (Li^+) including the electron loss to the continuum is studied. The present model takes account of the two-center effect on the ejected electron which is crucial for a proper description of the projectile ionization involving an ionic target. Both the triply differential cross section and the doubly differential cross section (DDCS) (energy spectra) are investigated at intermediate and high incident energies for the target elastic case. A broad distinct electron-loss peak (ELP) centered around $v_e \approx v_p$ is noted in the electron energy spectrum in contrast to the sharp ELP for a heavy projectile. Two salient features are noted in the present study: (i) the shift of the e DDCS peak (summed over e^+ angles) toward higher ejection energy with respect to half the residual energy of the system and (ii) comparison of the e and e^+ energy spectra reflects a strong e-e^+ asymmetry with respect to the ratio v_e(velocity of e)/v_p(velocity of e^+)=1. Both these features could be attributed to the postcollisional two-center effect on the e due to its parent nucleus (e^+) and the screened target ion. Two different wave functions of the Li ion are chosen in order to test the sensitivity of the present results with respect to the choice of the wave function.

DOI: 10.1103/PhysRevA.80.022713 PACS number(s): 34.90.+q, 36.10.−k

I. INTRODUCTION

Electron emission process in atom-atom or ion-atom collisions becomes particularly interesting at the same time complex when a structured projectile loses electron in collision with the target. Two independent channels can contribute to such projectile electron-loss process, e.g., the projectile electron can be knocked out by the screened target nucleus or by a target electron [1]. In the former process (singly inelastic) the target usually remains in its ground state, i.e., target elastic while in the latter (doubly inelastic), the target gets excited or ionized, i.e., target inelastic. Since these two channels lead to different final products, their contributions are to be added incoherently (i.e., in the cross-section level). The relative importance of the two channels depends on the incident energy as well as on the particular collision system.

Most of the earlier experiments [2–10] and consequently theories [11–14] on the projectile ionization concentrated on bare, partially stripped [2–6,8–14] or neutral heavy projectiles [7] for which a distinct signature of a cusp or peak was observed in the emitted electron energy spectrum at around v_e (velocity of the electron) $\approx v_p$ (velocity of the positron). This peak was attributed to the electron loss from the projectile ion/atom into its low-lying continuum, usually referred to as the electron-loss peak (ELP). With the advent of monoenergetic energy tunable positronium (Ps) beams [15,16], attention is also being focused experimentally [17] on the breakup process of light projectile, e.g., Ps atom.

The basic difference between the heavy projectile and the light projectile fragmentation is that, in the former case the deflection as well as the energy loss of the projectile, due to its heavy mass is negligibly small leading to a pronounced peak or cusp in the forward direction, while in the latter case, the light projectile can scatter to large angles and its energy loss is also not negligible leading to a broad peak or cusp. The study of the dynamics, e.g., angular and energy distributions of the process gives valuable information about the ionizing mechanisms and provides a unique insight into the collision dynamics as well as the atomic structure of the collision partners.

The Ps atom is now considered to be an ideal probe to solid surfaces for determining their structures mainly because it can only undergo elastic reflection from the outer surface layer of a solid [18]. Because of the large break-up probability of the Ps (above its binding energy 6.8 eV), the multiple scattering effect from inner-layer atoms of the solid is expected to be negligible for the Ps (unlike the low-energy electron and positron) and as such the low-energy Ps collision should be confined to the outer most surface layers. However, neutral atoms and molecules such as He and H_2 also interact mainly with the surface atoms, but the available low-energy beams are not energetic enough to probe small scale surface structure [19,20]. Thus the Ps provides a great deal of advantage over charged as well as neutral heavy projectiles as a probe to study the structure of atoms and molecules and the surface properties of solids and the knowledge of different scattering parameters for Ps [21–25]—atom, molecule, or ion collisions could be highly useful for such studies. Further, by virtue of very light mass of Ps (three orders of magnitude smaller than hydrogen), its interaction with various forms of matter, ranging from electrons, protons, alkali ions to atoms, molecules, solid surfaces, and plasmas can provide important information about the target medium.

In an earlier work [26] we developed a quantum-mechanical approach to study the breakup of Ps in collision with a hydrogenic ion (He^+) where the results showed prominent signature of the two-center effect [27–29] on the ejected electron in the final channel. The present work addresses the extension of it [26] to a more complex system, e.g., the two-electron (helium like) ionic target, Li^+ for the target elastic case;

$$\text{i.e.,} \quad e^+ e(1s) + \mathrm{Li}^+(1s) \rightarrow e^- + e^+ + \mathrm{Li}^+(1s). \qquad (1)$$

One major advantage of the Li^+ target (over He^+) is that the electrons of the former are much more tightly bound than the electron of the Ps atom and as such the probability of the electron loss from the projectile Ps is expected to be much higher than the ionization of the target. Further, in view of the large excitation energy of the target Li^+ as compared to the projectile Ps, we have neglected any virtual or real excitation of the Li^+ target during the fragmentation, i.e., only the target elastic case is considered.

Since the initial components of reaction (1) are both composite bodies, the theoretical prescription of such a process is rather complicated. As such one has to resort to some simplifying assumptions for the theoretical modeling of such a many-body (five body) reaction process. The present calculation is performed in the frame work of the postcollisional Coulomb distorted eikonal approximation (CDEA) taking account of the proper asymptotic three body boundary condition in the final channel, which is one of the important criteria for a reliable estimate of the ionization cross sections. The present work is a theoretical attempt [30] for the Ps breakup with a two-electron ionic target.

II. THEORY

The prior form of the ionization amplitude for the aforesaid process [Eq. (1)] is given as

$$T_{if}^{prior} = \langle \Psi_f^-(\vec{r}_1,\vec{r}_2,\vec{r}_3,\vec{r}_4)|V_i|\psi_i(\vec{r}_1,\vec{r}_2,\vec{r}_3,\vec{r}_4)\rangle, \tag{2}$$

where $\vec{r}_1$, $\vec{r}_2$, $\vec{r}_3$, and $\vec{r}_4$ are the position vectors of the positron and the electron of the positronium atom and the bound electrons of the Li^+ ion, respectively, with respect to the target nucleus

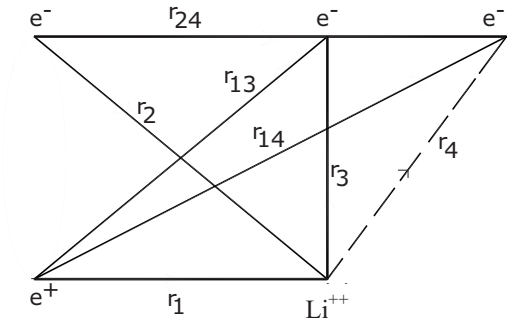

V_i is the initial channel perturbation and can be given by

$$V_i = \frac{Z_t}{r_1} - \frac{Z_t}{r_2} - \frac{1}{r_{13}} + \frac{1}{r_{23}} - \frac{1}{r_{14}} + \frac{1}{r_{24}}, \tag{3}$$

with Z_t (=3) being the charge of the target nucleus; $\vec{r}_{13}=\vec{r}_1-\vec{r}_3$, $\vec{r}_{23}=\vec{r}_2-\vec{r}_3$, $\vec{r}_{14}=\vec{r}_1-\vec{r}_4$, and $\vec{r}_{24}=\vec{r}_2-\vec{r}_4$.

The initial asymptotic state ψ_i in Eq. (2) is chosen as

$$\psi_i = \phi_{Ps}(|\vec{r}_1+\vec{r}_2|)e^{i\vec{k}_i\cdot\vec{R}}\phi_{Li^+}(\vec{r}_3,\vec{r}_4), \tag{4a}$$

where $\vec{R}=(\vec{r}_1+\vec{r}_2)/2$ and $\vec{k}_i$ is the initial momentum of the Ps atom with respect to the target nucleus. The ground-state wave function of the Ps atom $\phi_{Ps}(|\vec{r}_1-\vec{r}_2|)$ is given by

$$\phi_{Ps}(|\vec{r}_1-\vec{r}_2|) = N_{Ps}\exp(-\lambda_{Ps}r_{12}),$$

$$\text{with } N_{Ps}=\lambda_{Ps}^{3/2}/\sqrt{\pi} \text{ and } \lambda_{Ps}=1/2. \tag{4b}$$

Two different forms of the ground-state wave function [31–33] for Li^+ ion are chosen:

(i) Due to Morse *et al.* [31,32]:

$$\phi_{Li^+}(r_3,r_4) = u(r_3)u(r_4), \tag{5a}$$

where,

$$u(r) = \sqrt{\lambda_{Li^+}^3/\pi}\exp[-\lambda_{Li^+}(r)], \tag{5b}$$

with

$$\lambda_{Li^+} = (Z_t-1)+0.6875, \tag{5c}$$

ground-state energy $(E_0)=-7.222\ 656$ a.u.

(ii) Due to Clementi and Roetti (CR) [33]:

$$\phi_{Li^+}(r_3,r_4) = u(r_3)u(r_4), \tag{6a}$$

with

$$u(r) = \frac{1}{\sqrt{4\pi}}[N_1C_1\exp(-2.450\ 55\ \ r) + N_2C_2 \times\exp(-4.572\ 59\ \ r) + N_3C_3\exp(-6.670\ 32\ \ r)], \tag{6b}$$

where,

$$N_1 = 7.672\ 296,\ \ N_2 = 19.557\ 01,\ \ N_3 = 34.454\ 821,$$

$$C_1 = 0.890\ 66,\ \ C_2 = 0.123\ 28,\ \ C_3 = 0.000\ 88, \tag{6c}$$

where $E_0=-7.236\ 41$ a.u.; the accurate value of energy being [34] -7.2777 a.u.

Since the energies of the above two wave functions [31–33] are quite close to the very accurate value of the energy [34], both wave functions are considered to be good enough, the CR [33] being better than the Morse [31,32] one.

To construct the final channel wave function one should note that the ejected electron is in the combined (attractive) fields of the two positive ions, e.g., its parent ion e^+ and the target ion Li^+. The present model takes account of this two-center effect and the final-state wave function Ψ_f^- in Eq. (2) satisfying the incoming wave boundary condition is approximated by the following ansatz in the framework of coulomb modified eikonal approximation [26,35]

$$\Psi_f^-(\vec{r}_1,\vec{r}_2,\vec{r}_3,\vec{r}_4) = (2\pi)^{-3}N_{Li^+}\exp(-\lambda_{Li^+}r_3) \times\exp(-\lambda_{Li^+}r_4)e^{i\vec{k}_1\cdot\vec{r}_1}e^{i\vec{k}_2\cdot\vec{r}_2}{}_1F_1 \times[-i\alpha_2,1,-i(k_2r_2+\vec{k}_2\cdot\vec{r}_2)] \times\exp\left[i\eta_1\int_z^\infty\left(\frac{1}{r_1}-\frac{1}{r_{12}}\right)dz'\right], \tag{7}$$

with $\alpha_2=-(Z_t-2)/k_2$ and $\eta_1=(Z_t-2)/k_1$; $\vec{k}_1$ and $\vec{k}_2$ being the final momenta of the scattered positron and the ejected electron with respect to the target nucleus, respectively.

The eikonal phase integral [35] occurring in Eq. (7) arises due to the distortion of the outgoing positron $(\vec{r}_1)$ in the field

of the screened target nucleus Li^+ as well as of the continuum electron ($\vec{r}_2$). The latter takes some account for the Ps continuum. It should be mentioned here that the present model neglects the effect of excited Ps states which could probably be incorporated in more sophisticated theories, e.g., through coupled channel calculations [36]. In fact, the inclusion of these Ps states might play an important role in the Ps break-up process [36].

In view of Eqs. (2), (3), (4a), (4b), and (5a)–(5c) we get the break-up amplitude:

$$T_{if} \approx -\frac{\mu_f}{2\pi}\int\int\int N_{\mathrm{Li}^+}\exp(-\lambda_{\mathrm{Li}^+}r_3)e^{-i\vec{k}_1\cdot\vec{r}_1} \times e^{-i\vec{k}_2\cdot\vec{r}_2}{}_1F_1(i\alpha_2,1,i(k_2r_2+\vec{k}_2\cdot\vec{r}_2))(r_1+z_1)^{i\eta_1} \times (r_{12}+z_{12})^{-i\eta_1}\left(\frac{Z_t}{r_1}-\frac{Z_t}{r_2}-\frac{1}{r_{13}}+\frac{1}{r_{23}}-\frac{1}{r_{14}}+\frac{1}{r_{24}}\right) \times N_{\mathrm{Ps}}\exp(-\lambda_{\mathrm{Ps}}r_{12})N_{\mathrm{Li}^+}\exp(-\lambda_{\mathrm{Li}^+}r_4)d\vec{r}_1d\vec{r}_2d\vec{r}_3d\vec{r}_4. \tag{8}$$

After much analytical reduction [37,38] the break-up amplitude T_{if} in Eq. (8) is finally reduced to a two-dimensional numerical integral [39]. The triply differential cross section (TDCS) for the break-up process is given by

$$\frac{d^3\sigma}{dE_2d\Omega_1d\Omega_2}=\frac{k_1k_2}{k_i}|T_{if}|^2. \tag{9}$$

The corresponding expression for the double differential cross section (DDCS) is obtained by integrating the TDCS in Eq. (9) over the solid angles of the e or the e^+ and is given by

$$\frac{d^2\sigma}{dE_2d\Omega_1(d\Omega_2)}=\frac{k_1k_2}{k_i}\int|T_{if}|^2d\Omega_2(d\Omega_1), \tag{10}$$

where Ω_1 and Ω_2 are the solid angles corresponding to the coordinates $\vec{r}_1$ and $\vec{r}_2$, respectively, and is given by

$$\Omega=\sin\theta d\theta d\phi. \tag{11}$$

III. RESULTS AND DISCUSSIONS

We have computed the fully TDCSs as well as the DDCSs for the ionization of Ps atom in collision with the heliumlike ionic target (e.g., Li^+) for the target elastic case. Since the present study is being made in coplanar geometry, i.e., $\vec{k}_i$, $\vec{k}_1$, and $\vec{k}_2$ all being in the same plane, the azimuthal angles ϕ_1 and ϕ_2 can assume values, $\phi_1=0°$, $\phi_2=0°$, and 180°. For the TDCS curves, we have adopted the following conventions for the ejected angles (θ_2,ϕ_2): for $(\theta_2,0°)$ we have denoted

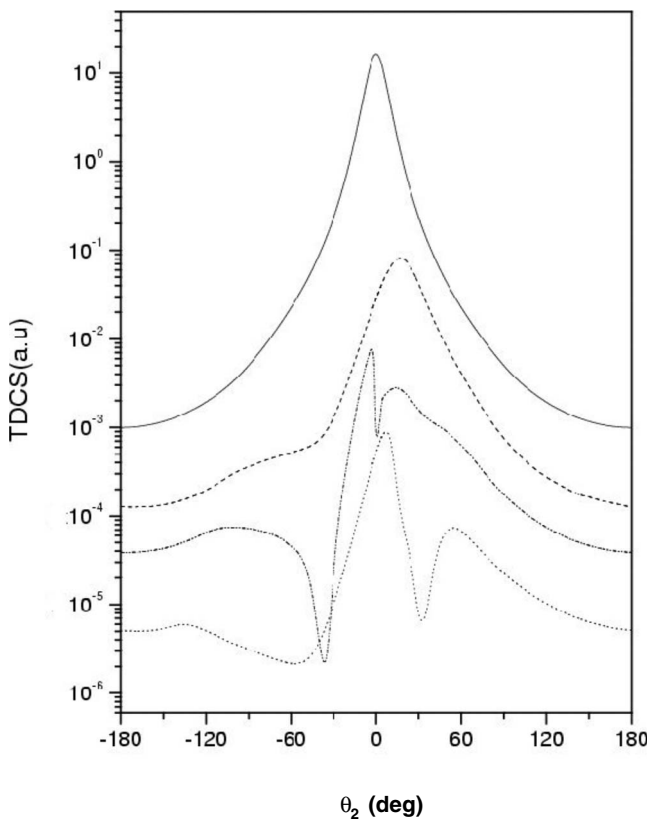

FIG. 1. The TDCSs against the ejected electron angle (θ_2) for different values of the scattered positron angle (θ_1). The incident energy (E_i) is fixed at 50 eV, ejected electron energy (E_2) is fixed at 17 eV. The solid curve for $\theta_1=0°$, dashed curve for $\theta_1=20°$, dashed dot-dot curve represents $\theta_1=30°$, and the dotted curve for $\theta_1=45°$.

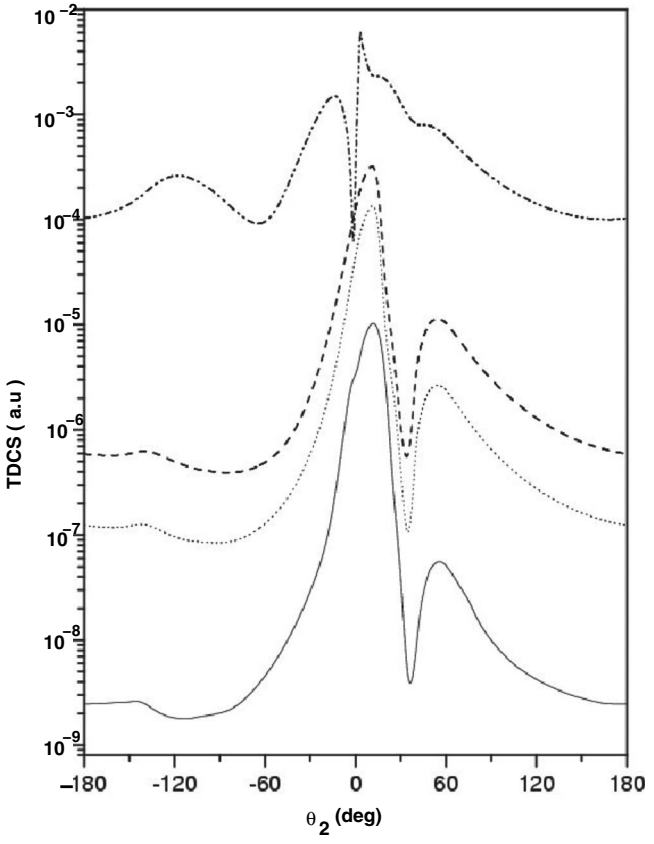

FIG. 2. TDCS against the ejected electron angle (θ_2) for different incident energies but for $\theta_1=45°$. Dashed double dot curve for $E_i=25$ eV, $E_2=8$ eV; dashed curve for $E_i=75$ eV, $E_2=28$ eV; dotted curve for $E_i=100$ eV, $E_2=40$ eV; and solid curve for $E_i=200$ eV, $E_2=90$ eV.

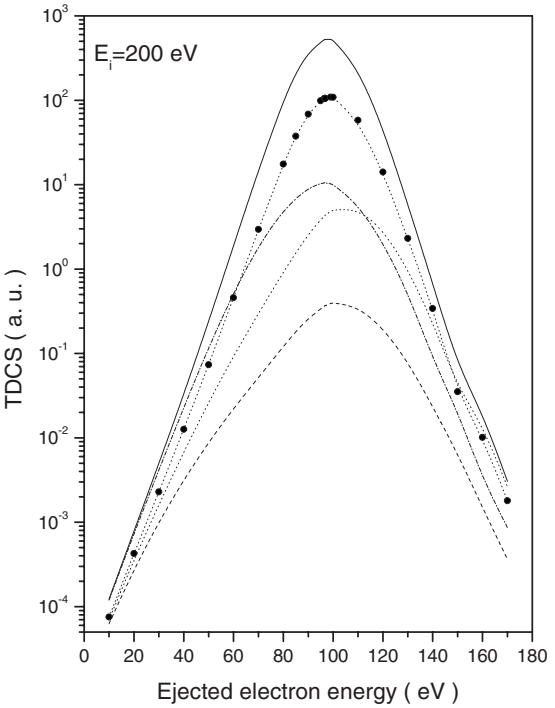

FIG. 3. TDCS against the ejected electron energy (E_2) for E_i =200 eV. Solid curve for $\theta_1=\theta_2=0°$; dotted curve with solid circles for $\theta_1=-\theta_2=5°$; dash dot curve for $\theta_1=0°$, $\theta_2=5°$; dotted curve for $\theta_1=5°$, $\theta_2=0°$; and dashed curve for $\theta_1=\theta_2=5°$.

by $-|\theta_2|$ (recoil region), while the angles $(\theta_2, 180°)$ are plotted as $|\theta_2|$ (binary region).

Figure 1 display the TDCSs against the ejected electron angle (θ_2) at an incident energy $E_i=50$ eV, with some selected values of the scattering angle (e.g., $\theta_1=0°$, 20°, 30°, 45°) of the positron. The TDCS (Fig. 1) exhibits a broad ELP for forward emission (0°) of both the e and the e^+ in contrast to the sharp cusp (ELP) around 0° for heavy-ion impact [7]. This could be attributed to the probability of deflection of the light particle (e^+) to higher angles in contrast to the heavy projectile which due to its heavy mass is predominantly scattered in the forward direction (0°). Further, as is evident from Fig. 1 that the TDCS exhibits some asymmetry in the shape of the binary and recoil regions with increasing scattering angles and the cross section decreases throughout the angular region with increasing scattering angle. A prominent double peak structure appears (in the binary region) particularly at $\theta_1=45°$, the explanation of which will be discussed below.

For the confirmation of the above behavior, we have presented in Fig. 2 the TDCS vs θ_2 for $\theta_1=45°$ at different incident energies. The occurrence of the distinct double peak particularly at 45° could be attributed to the higher-order effects considered in the present model. This could also be associated with the famous Thomas (p-n-e) mechanism (TM) [40,41] in charge-transfer problems at high incident energies. Figure 2 also reflects that the secondary peak becomes more and more prominent with increasing incident energy, indicating the importance of the higher-order effects at higher incident energies.

Figure 3 demonstrates the ejection energy distribution

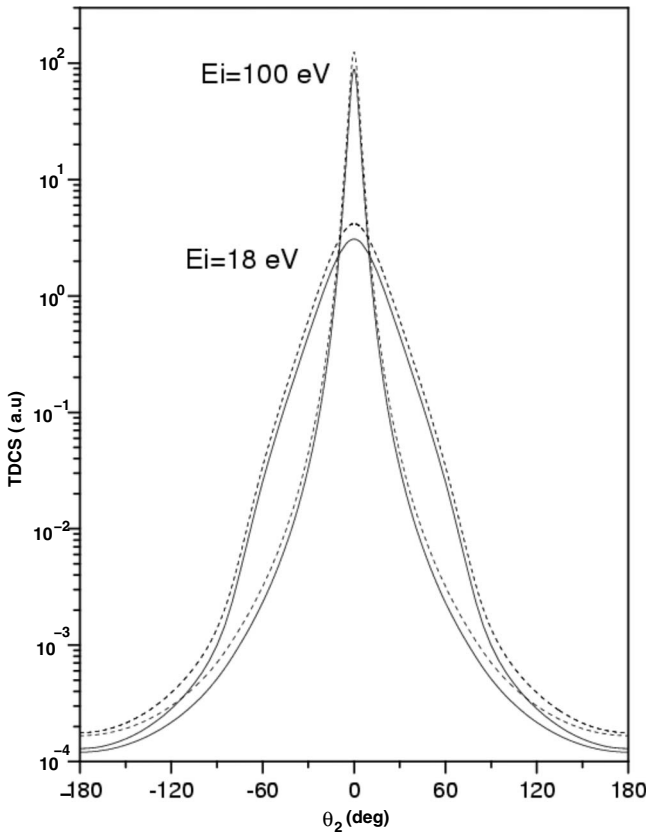

FIG. 4. TDCS using different ground-state wave functions of Li ion at $E_i=18$ and 100 eV. Solid lines for simple Morse [31,32] wave function and dashed lines for CR wave functions [33].

(TDCS) of the e at an incident energy $E_i=200$ eV for different combinations of the ejection and scattering angles. The azimuthal angles are chosen as $\phi_1=\phi_2=0°$, i.e., when the scattered positron and ejected electron emerge on the same side of the incident beam. The following important features are noted in Fig. 3 which gives a clear indication of the post collisional two-center effect [27–29]:

(i) The energy spectrum (TDCS) exhibits a broad peak (unlike the heavy projectile) at slightly above half of the residual energy ($E_{res}/2$) with some exception (dashed dotted curve) to be described below. The broadness being decreased with decreasing ejection angles and magnitude of the TDCS peak is enhanced with decreasing ejection angles as is expected physically.

(ii) When the e^+ angle (θ_1) is greater than the e angle (θ_2) the TDCS peak shifts toward the higher ejection energy with respect to $E_{res}/2$. While, the reverse behavior is noted when $\theta_2>\theta_1$, i.e., the peak shifts toward lower energy in this case. This shifting of the TDCS peak could be attributed to the postcollisional two-center effect on the ejected e due to the e^+ and the target nucleus. Higher ejection angle (θ_2) of e corresponds to lower ejection energy (E_2) while higher scattering angle (θ_1) of e^+ corresponds to lower e^+ energy (E_1), i.e., higher E_2, as the residual energy E_{res} is shared by the e^+ and the e if the recoil of the target ion is neglected.

In order to test the sensitivity of the present results with respect to the choice of the target wave functions we have depicted in Fig. 4 the TDCS corresponding to the two differ-

TABLE I. Differential cross sections (in a.u.) using the CR [33] wave function. The values within brackets indicate the power of 10.

Angle (deg)	Energy (eV) 25	50	100	200
0	1.04[+1]	4.31[+1]	1.73[+2]	7.12[+2]
10	6.19[+0]	7.73[+0]	3.86[+0]	1.28[+0]
20	2.19[+0]	1.08[+0]	3.43[−1]	1.08[−1]
30	7.75[−1]	2.69[−1]	7.98[−2]	2.55[−2]
40	3.05[−1]	9.39[−2]	2.83[−2]	9.13[−3]
50	1.29[−1]	4.06[−2]	1.27[−2]	4.16[−3]
60	5.76[−2]	2.01[−2]	6.62[−3]	2.23[−3]
70	2.54[−2]	1.08[−2]	3.84[−3]	1.33[−3]
80	1.14[−2]	6.15[−3]	2.41[−3]	8.64[−4]
90	6.58[−3]	3.73[−3]	1.59[−3]	5.98[−4]
100	3.52[−3]	2.51[−3]	1.13[−3]	4.38[−4]
110	2.39[−3]	1.82[−3]	8.52[−4]	3.38[−4]
120	1.76[−3]	1.41[−3]	6.75[−4]	2.74[−4]
130	1.37[−3]	1.14[−3]	5.59[−4]	2.29[−4]
140	1.12[−3]	9.62[−4]	4.81[−4]	2.01[−4]
150	9.67[−4]	8.48[−4]	4.29[−4]	1.80[−4]
160	8.71[−4]	7.76[−4]	3.96[−4]	1.67[−4]
170	8.19[−4]	7.35[−4]	3.78[−4]	1.60[−4]
180	8.02[−4]	7.22[−4]	3.72[−4]	1.58[−4]

ent wave functions [31–33] for the target Li^+ ion at a low (18 eV) and a high (100 eV) incident energies. The difference between the two curves is more prominent at lower incident energy as well as at backward angles (the CR being always higher) and tend to die out with increasing energy so that at $E_i=100$ eV the deviation is almost negligible, particularly at forward angles. However it should be pointed out that due to the logarithmic scale in Fig. 4, the real difference between the two results (CR and Morse) is not quite apparent. In fact the two TDCS results differ by around 34–35 % which is quite significant especially at lower energies. Since the computation using the CR wave function [33] is more time consuming, we have mostly used the simpler Morse wave function [31,32] particularly for higher incident energies where the sensitivity with respect to the wave function is quite small. Some numerical values of the fragmentation TDCS using the CR wave function [33] are tabulated in Table I.

Figure 5 demonstrates the electron energy distribution (DDCS) at an incident energy $E_i=50$ eV where the DDCS refers to the summation over the positron scattering angles ($\Sigma\theta_1$, ϕ_1, henceforth referred to as electron DDCS) for different ejection angles θ_2. The inset exhibits the corresponding e^+ energy spectrum of the same DDCS (i.e., $\Sigma\theta_1$, ϕ_1). The DDCS corresponding to the CR wave function [33] for 0° emission of e is also included in Fig. 5. As is apparent from the figure, the DDCS exhibits a broad peak (similar to the TDCS one), slightly shifted toward higher ejection energy with respect to $E_{res}/2$. However, this shift decreases and moves toward $E_{res}/2$ with increasing ejection angle (θ_2). This is because the lower-energy electron is preferentially

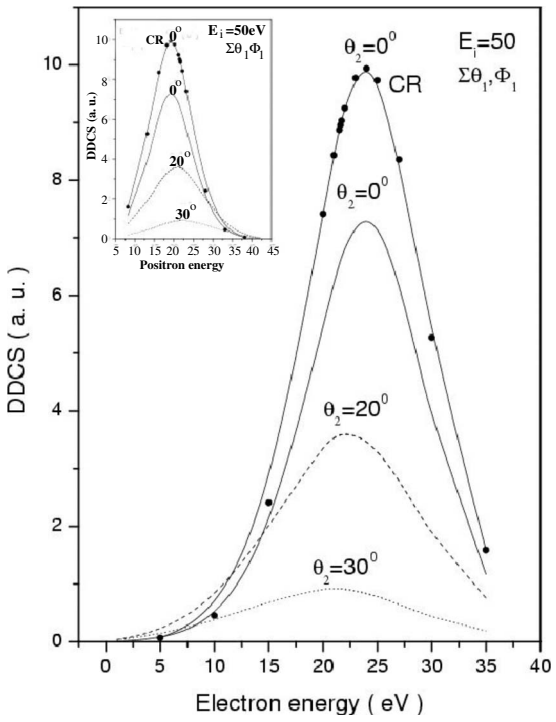

FIG. 5. The electron DDCS ($\Sigma\theta_1$, ϕ_1) against the ejected e energy for different values of the ejected e angle (θ_2) at the fixed incident energy ($E_i=50$ eV). The solid curve is for $\theta_2=0°$, dashed curve is for $\theta_2=20°$, and the dotted curve is for $\theta_2=30°$. Solid curve with circle corresponds to CR wave function [33] for $\theta_2=0°$. Both the curves for $\theta_2=0°$ are scaled down by five factor. The inset describes the same DDCS as in Fig. 5 but against the ejected e^+ energy.

ejected at higher angles (θ_2) so that finally at $\theta_2=30°$, the peak occurs exactly at $E_{res}/2$ (i.e., 21.6 eV). The broadness of the DDCS peak clearly reveals that the positron in the final state could also suffer some deflections to larger angles apart from the dominant forward scattering ($\theta_1=0°$). This is in contrast to the heavy projectile which due to its heavy mass is scattered only through forward angles giving rise to a sharp cusp in the ejected electron energy spectrum. The shifting of the DDCS peak ($\Sigma\theta_1$, ϕ_1) toward higher e ejection energy could be attributed to the same fact (two-center effect) described for the TDCS.

As regards the sensitivity of the DDCS with respect to the target wave function, the qualitative behavior of the two curves (CR and Morse wave functions) are more or less similar in nature (vide Fig. 5) although a significant quantitative difference (~36%) is noted particularly between the two peak values.

The positron DDCS summed over the electron ejection angles ($\Sigma\theta_2$, ϕ_2) is displayed in Fig. 6 against the e energy, while the inset represents the same against the e^+ energy. In this case, the DDCS peak shifts in the reverse direction (cf. Fig. 5 and inset), e.g., at slightly below $E_{res}/2$ for forward e^+ scattering ($\theta_1=0°$). Further, in contrast to Fig. 5, the peak shifts toward higher ejection energy for larger positron angle (θ_1). This behavior could be explained physically as follows. The e^+ DDCS (Fig. 6) includes the contributions from all the higher ejection angles (θ_2) of the e apart from the dominant

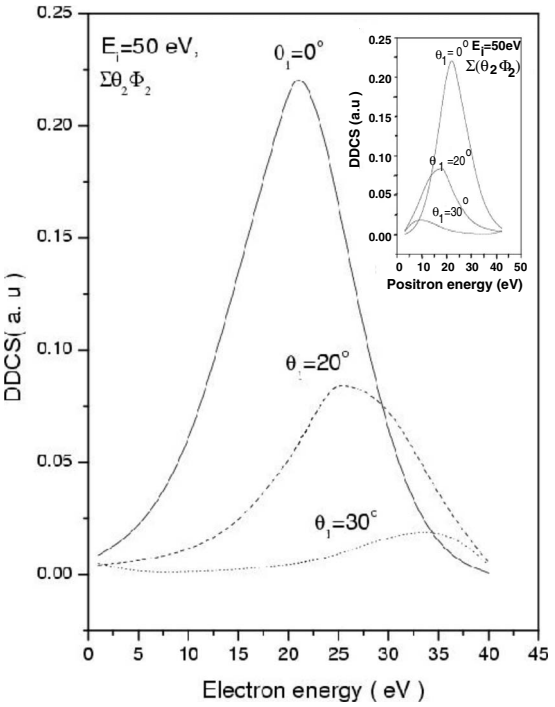

FIG. 6. The positron DDCS ($\Sigma\theta_2$, ϕ_2) against the ejected e energy for different values of the scattered e^+ angle (θ_1) at the fixed incident energy (E_i=50 eV). The solid curve is for θ_1=0°, dashed curve is for θ_1=20°, and the dotted curve is for θ_1=30°. Solid curve is scaled down by ten factor. The inset describes the same DDCS as in Fig. 5 but against the ejected e^+ energy.

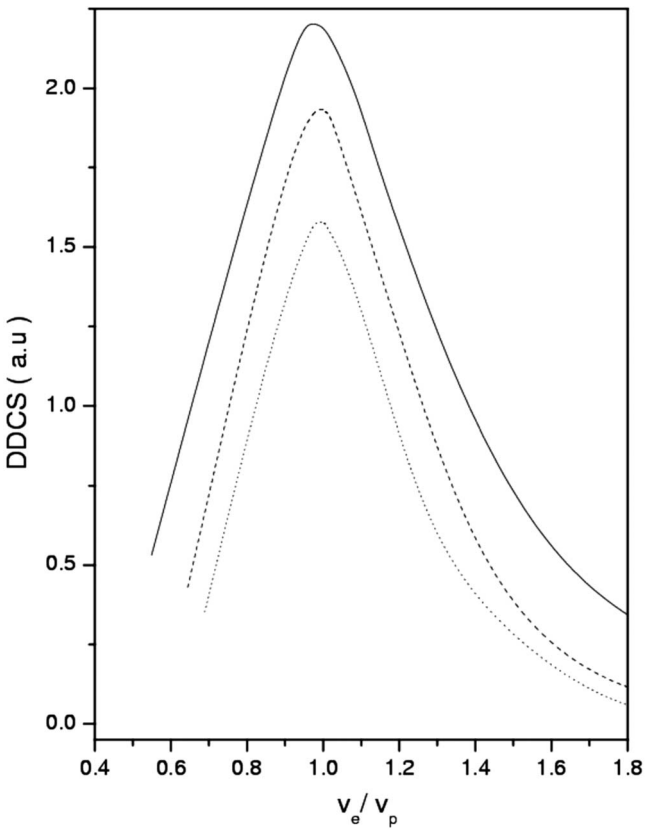

FIG. 7. The positron DDCS ($\Sigma\theta_2$, ϕ_2) is plotted against the ratio of v_e/v_p for three different incident energies. The scattered positron angle θ_1 is fixed at 0°. The solid curve is for E_i=50 eV, dashed curve is for E_i=75 eV, and the dotted curve is for E_i=100 eV.

forward emission (θ_2=0°) and higher emission angle corresponds to lower emission energy. Further, the lower e^+ energy corresponds to higher e energy and vice versa.

The dominance of the DDCS values for θ_2=0° in Fig. 5 and for θ_1=0° in Fig. 6 indicates that the ELP occurs when both the e^+ and the e are preferentially scattered in the forward direction. This could probably be ascribed to the following fact. The ELP arises when the electron and the positron are very close to each other in the velocity space. Thus the DDCS (energy distribution) maximizes at around half the residual energy $\sim E_{\text{res}/2}$ and for equal angles when both the particles move in the forward directions. In fact for heavy particle [7] impact a sharp ELP is noted at exact forward scattering (0°), while for light projectile (Ps), the ELP peak is comparatively broad (because of the light mass) although the maximum value occurs at exact zero degree.

Finally Fig. 7 displays the positron DDCS against the ratio $R=v_e/v_p$ for forward scattering (θ_1=0°) at three different incident energies. Figure 7 clearly demonstrates that the DDCS peak occurs at a lower ratio of v_e/v_p than unity (i.e., $v_e/v_p<1$). Further, the position of the peak shifts gradually toward a higher value of R with increasing incident energy, e.g., R being 0.97 at E_i=50 eV and attains a value of almost unity ($R\sim1.006$) at E_i=100 eV (vide Fig. 7). A plausible physical explanation for the above behavior could be as follows. In the postcollisional interaction, the e and the e^+ are distorted by their increasing interactions with the target. Since the e^+ feels repulsion while the e feels attraction due to the short range interaction with the target nucleus, on an average the e remains closer to the target while the e^+ moves away from it. As such, the probability of the e (e^+) to suffer hard (soft) collisions with the target increases with decreasing incident energy. Thus in the postcollisional effect, the electron is in the combined field of its parent (e^+) and the target nucleus.

IV. CONCLUSIONS

The salient features of the present study are outlined below:

(1) The angular distribution of the e (TDCS) exhibits a sharp peak (ELP) at around half the residual energy ($E_{res}/2$) with diminishing magnitude for higher e^+ scattering angles.

(2) The ELP exhibits a spread in the velocity space around $\vec{v}_e=\vec{v}_p$ for forward emission of the e/e^+, unlike the sharp cusp (ELP) around 0° for heavy-ion impact. The reason being, in contrast to the case of heavy-ion impact, the e and the e^+ due to their light mass could suffer considerable deflection from their initial velocities.

(3) The occurrence of a distinct double peak in the e (θ_2) distribution (exactly at θ_1=45°) as well as its becoming more and more prominent with increasing incident energy could be attributed to higher-order effects and could possibly be associated with the famous Thomas mechanism.

(4) A notable shift of the DDCS peak in the e DDCS (to higher momenta) from its standard position ($\vec{v}_e=\vec{v}_p$) is ob-

tained. The e^+ DDCS shows exactly the reverse behavior as expected.

(5) The position of the e^+ DDCS peak shifts gradually toward higher value of the ratio v_e/v_p with increasing incident energy.

(6) The sensitivity of the ground-state wave function of Li ion is quite significant being more at low incident energies, the results being higher for better wave function (CR).

Finally, we would like to comment that the present results might change considerably (both qualitatively and quantitatively) if an improved scattering wave function, particularly incorporating the Ps excited states including the Ps continuum could be used in the T matrix, i.e., in the frame work of coupled channel calculations.

[1] D. R. Bates and G. W. Griffing, Proc. Phys. Soc., London, Sect. A **67**, 663 (1954).
[2] G. B. Crooks and M. E. Rudd, Phys. Rev. Lett. **25**, 1599 (1970).
[3] D. Burch, H. Wieman, and W. B. Ingalls, Phys. Rev. Lett. **30**, 823 (1973).
[4] D. H. Lee, P. Richard, T. J. M. Zouros, J. M. Sanders, J. L. Shinpaugh, and H. Hidmi, Phys. Rev. A **41**, 4816 (1990).
[5] N. Stolterfoht, R. D. DuBois, and R. D. Riverolla, *Electron Emission in Heavy Ion Atom Collisions*, Springer Series on Atoms and Molecules (Springer, New York, 1997).
[6] B. B. Dhal, L. C. Tribedi, U. Tiwari, K. V. Thulasiram, P. N. Tandon, T. G. Lee, C. D. Lin, and L. Gulyas, Phys. Rev. A **62**, 022714 (2000).
[7] M. B. Shah, C. McGrath, C. Illescas, B. Pons, A. Riera, H. Luna, D. S. F. Crothers, S. F. C. O'Rourke, and H. B. Gilbody, Phys. Rev. A **67**, 010704(R) (2003).
[8] D. Misra, U. Kadhane, Y. P. Singh, L. C. Tribedi, P. D. Fainstein, and P. Richard, Phys. Rev. Lett. **92**, 153201 (2004).
[9] A. H. Kelkar, D. Misra, and L. C. Tribedi, J. Phys.: Conf. Ser. **80**, 012010 (2007).
[10] D. Misra, A. Kelkar, U. Kadhane, A. Kumar, Y. P. Singh, L. C. Tribedi, and P. D. Fainstein, Phys. Rev. A **75**, 052712 (2007).
[11] D. Schneider, M. Prost, N. Stolterfoht, G. Nolte, and R. Du Bois, Phys. Rev. A **28**, 649 (1983).
[12] H. Atan, W. Steckelmacher, and M. W. Lucas, J. Phys. B **23**, 2579 (1990).
[13] J. Wang, C. O. Reinhold, and J. Burgdörfer, Phys. Rev. A **44** 7243 (1991).
[14] I. F. Barna, A. C. Gagyi-Palffy, L. Gulyas, K. Tokesi, and J. Burgdorfer, Nucl. Instrum. Methods Phys. Res. B **233**, 176 (2005).
[15] A. J. Garner, A. Özen, and G. Laricchia, J. Phys. B **33**, 1149 (2000).
[16] A. Özen, A. J. Garner, and G. Laricchia, Nucl. Instrum. Methods Phys. Res. B **171**, 172 (2000).
[17] S. Armitage, D. E. Leslie, A. J. Garner, and G. Laricchia, Phys. Rev. Lett. **89**, 173402 (2002).
[18] K. F. Canter, in *Positron Scattering in Gases*, edited by J. W. Humberston and M. R. C. McDowell (Plenum, New York, 1984) p. 219.
[19] M. H. Weber, S. Tang, S. Berko, B. L. Brown, K. F. Canter, K. G. Lynn, A. P. Mills, Jr., L. O. Roellig, and A. J. Viescas, Phys. Rev. Lett. **61**, 2542 (1988).
[20] P. K. Biswas and S. K. Adhikari, Phys. Rev. A **59**, 363 (1999).
[21] N. K. Sarkar, P. Chaudhury, and A. S. Ghosh, J. Phys. B **32**, 1657 (1999).
[22] S. Chakraborty and A. S. Ghosh, Phys. Rev. A **72**, 052508 (2005).
[23] P. K. Sinha, P. Chaudhuri, and A. S. Ghosh, Phys. Rev. A **69**, 014701 (2004).
[24] P. Van Reeth and J. W. Humberston, Nucl. Instrum. Methods Phys. Res. B **221**, 140 (2004).
[25] N. Stolterfoht, H. Platten, G. Schiwietz, D. Schneider, L. Gulyas, P. D. Fainstein, and A. Salin, Phys. Rev. A **52**, 3796 (1995).
[26] S. Roy, D. Ghosh, and C. Sinha, J. Phys. B **38**, 2145 (2005).
[27] L. C. Tribedi, P. Richard, Y. D. Wang, C. D. Lin, L. Gulyas, and M. E. Rudd, Phys. Rev. A **58**, 3619 (1998).
[28] L. C. Tribedi, P. Richard, L. Gulyas, M. E. Rudd, and R. Moshammer, Phys. Rev. A **63**, 062723 (2001).
[29] D. Misra, A. Kumar, U. R. Kadhane, P. D. Fainstein, and L. C. Tribedi, Radiat. Phys. Chem. **75**, 1723 (2006).
[30] S. Roy and C. Sinha, e-print arXiv:0808.3096.
[31] P. M. Morse, L. A. Young, and E. S. Haurwitz, Phys. Rev. **48**, 948 (1935).
[32] B. L. Moiseiwitsch and S. J. Smith, Rev. Mod. Phys. **40**, 238 (1968).
[33] E. Clementi and C. Roetti, At. Data Nucl. Data Tables **14**, 177 (1974).
[34] K. V. Rodriguez, G. Gasaneo, and D. M. Mitnik, J. Phys. B **40**, 3923 (2007) see also other references cited therein.
[35] F. W. Byron, Jr. and C. J. Joachain, Phys. Rep. **34**, 233 (1977).
[36] J. E. Blackwood, C. P. Campbell, M. T. McAlinden, and H. R. J. Walters, Phys. Rev. A **60**, 4454 (1999).
[37] R. Biswas and C. Sinha, Phys. Rev. A **50**, 354 (1994).
[38] B. Nath and C. Sinha, Eur. Phys. J. D **6**, 295 (1999).
[39] B. Nath and C. Sinha, J. Phys. B **33**, 5525 (2000).
[40] L. H. Thomas, Proc. R. Soc. London, Ser. A **114**, 561 (1927).
[41] D. Ghosh and C. Sinha, Phys. Rev. A **68**, 062701 (2003).